New semi-analytical method for fast transcranial ultrasonic field simulation

Célestine Angla, Hamza Chouh, Paul Mondou, Gwenael Toullelan, Kévyn Perlin, Vincent Brulon, Emmanuel de Schlichting, Benoit Larrat, Jean-Luc Gennisson, Sylvain Chatillon

New semi-analytical method for fast transcranial ultrasonic field simulation

C. Angla[1,4], H Chouh[1], P. Mondou[2], G Toullelan[1], K. Perlin[1], V. Brulon[4], E. De Schlichting[3], J.-L. Gennisson[4,*], B. Larrat[2,*], and S. Chatillon[1,*]

[1] Université Paris-Saclay, CEA List, F-91120, Palaiseau, France
[2] Université Paris-Saclay, CNRS, CEA, Neurospin 91191, Gif-sur-Yvette, France
[3] CHU Grenoble-Alpes, Service de Neurochirurgie, F-38700, Grenoble, France
[4] Université Paris-Saclay, CNRS, Inserm, CEA, BioMaps, 91190, Orsay, France
[*] co-last authors

E-mail: c-angla@orange.fr

Abstract. To optimize and ensure the safety of ultrasound brain therapy, personalized transcranial ultrasound simulations are very useful. They allow to predict the pressure field, depending on the patient skull and probe position. Most transcranial ultrasound simulations are based on numerical methods which have a long computation time and a high memory usage. The goal of this study is to develop a new semi-analytical field computation method that combines realism and computation speed.

Instead of the classic ray tracing, the ultrasonic paths are computed by time of flight minimization. Then the pressure field is computed using the pencil method. This method requires a smooth and homogeneous skull model. The simulation algorithm, so-called SplineBeam, was numerically validated, by comparison with existing solvers, and experimentally validated by comparison with hydrophone measured pressure fields through an *ex vivo* human skull.

SplineBeam simulated pressure fields were close to the experimentally measured ones, with a focus position difference of the order of the positioning error and a maximum pressure difference lower than 6.02%. In addition, for those configurations, SplineBeam computation time was lower than another simulation software, k-Wave's, by two orders of magnitude, thanks to its capacity to compute the field only at the focal spot.

These results show the potential of this new method to compute fast and realistic transcranial pressure fields. The combination of this two assets makes it a promising tool for real time transcranial pressure field prediction during ultrasound brain therapy interventions.

Keywords: Fast Transcranial Simulations, Skull Modeling, Ultrasound Brain Therapy

1. Introduction

Most drugs are ineffective for brain diseases because of the Blood-Brain-Barrier (BBB). Focusing low intensity ultrasound waves in the brain, combined with the injection of microbubbles in the blood vessels, allows to open the BBB. BBB opening [1] is an example of ultrasound use for brain therapy. Other examples include thermal ablation [2] and neuro-modulation [3]. All these therapies are non-invasive when the ultrasound waves are sent through the skull. However, the skull is a complex medium which strongly attenuates and aberrates the ultrasound beam. In addition, the geometric and acoustic properties of the skull vary between and within individuals, so the skull effects on the ultrasound propagation will be different depending on the patient and the probe position. Thus, to optimize and ensure the safety of transcranial ultrasound brain therapies, the pressure field can be predicted using personalized simulations. Most transcranial simulations are based on numerical methods, such as finite differences [4] or k-space [5], especially since the development of the Matlab toolbox k-Wave [6] in 2010. These methods take into account many complex physical phenomenons and allow a heterogeneous description of the skull [7]. However, they require a spatial step small enough to converge, making them quite slow and memory demanding. Even though the k-space method needs less spatial resolution to achieve convergence with reasonable accuracy than finite differences, it is still slower than ray-tracing by one order of magnitude [8]. On the other hand, semi-analytical methods, such as ray-tracing or the pencil method (developed in the CIVA Healthcare platform [9]), are believed to suffer from a lack of realism due to the approximations made and to the skull modeling which is often homogeneous and isotropic. However, this belief is debatable. Indeed, several studies compared the focus obtained through skulls by aberration correction using phase laws computed with semi-analytical and numerical methods. The results show that numerical method based phase correction outperforms ray-tracing based phase correction, but the gap between numerical methods and ray-tracing vary between the studies (ranging from a 2% difference [10] to a 50% difference [11] in restored pressure at focus). It means that semi analytical methods can be as accurate as numerical ones for aberration correction, depending on the method and skull model used. It suggests that for pressure field computation, semi-analytical could also reach equivalent accuracy as numerical methods, with a good method and an adapted skull model. However, it does not exist, to our knowledge, any study comparing pressure fields computed by semi-analytical and numerical methods with experimentally measured ones. In addition, Almquist et al. [12] showed that most of the accuracy of transcranial simulations relies on skull modeling. Thus, it is very likely that most semi analytical methods lacks of accuracy due to a too simple skull modeling, as they mostly use homogeneous skull models. The goal of this study was to develop a new semi-analytical transcranial ultrasound simulation method that combines realism and computation speed. To this aim, instead of 3D meshed surfaces, which are not suitable for the pencil model, we used splines to describe the skull surfaces in a smooth way, and instead of using a simple averaging method, we used the improved homogenization method developed in our previous study [13]. In addition, we developed a new path computation method, based on the minimization of the time of flight along a ray-path between a source point and the computation point. This allows to reduce the computation time, and to improve the pencil method by allowing a regular sampling of the transducer. We then compared the pressure fields simulated by this new semi-analytical method and those simulated by numerical methods with transcranial pressure fields measured by hydrophone.

2. Methods

2.1. Skull model

The skull is modeled as a homogeneous layer of bone, separated by two smooth interfaces.

2.1.1. Skull acoustic properties modeling The acoustic properties (density ρ and sound speed c) are derived from the skull CT scan using the formulas proposed by Marsac et al. [14]:

$$\rho = \rho_{\min} + (\rho_{\max} - \rho_{\min})\frac{HU - HU_{\min}}{HU_{\max} - HU_{\min}} \tag{1}$$

$$c = c_{\min} + (c_{\max} - c_{\min})\frac{\rho - \rho_{\min}}{\rho_{\max} - \rho_{\min}} \tag{2}$$

We use $HU_{\min} = HU_{\text{water}}$, where HU_{water} is taken as the average HU value of a region of the CT scan identified as water. $HU_{\max}$ is computed as the maximum value over the whole CT scan. The values used for $(\rho_{\min}, c_{\min}, \rho_{\max}, c_{\max})$ are given in table 1 and were taken from the literature [14].

Table 1: Extreme densities and sound speeds used in Marsac's formulas [14].

$\rho_{\min}$	$c_{\min}$	$\rho_{\max}$	$c_{\max}$
1000kg.m^{-3}	1500m.s^{-1}	2700kg.m^{-3}	4000m.s^{-1}

Then, instead of taking the average value on the CT scan to obtain a homogeneous medium, equivalent density and sound speed are computed with the homogenization method developed in our previous study [13]. In this method, the skull is first modeled as a three-layer medium (composed of two layers of cortical bone with a layer of trabecular bone in between), then an homogeneous isotropic equivalent medium is computed from the three-layer one. The equivalent sound speed is computed as the average sound speed, and the equivalent density is computed with an empirical formula that aims to compensate for the amplitude overestimation of the averaging method. The time of flight error between three-layer media and homogeneous media (with the average sound speed) was evaluated for different configurations (with trabecular bone sound speed varying from 2350m.s^{-1} to 2600m.s^{-1}, cortical bone sound speed varying from 2650m.s^{-1} to 2900m.s^{-1} and the percentage of trabecular bone varying from 0% to 90%). The mean and maximal errors for a realistic incidence angle distribution (obtained from a realistic transducer position relative to a skull) were respectively 0.27% and 0.39%.

The skull attenuation is modeled as a constant over the whole skull [15], but with a frequency dependency. As our simulation algorithm is based on a new method, we can not use any simulation-tuned formula from the literature, as the formula would probably depend on the attenuation phenomenons taken into account by the simulation method it was tuned with. Instead, we use an attenuation coefficient from a study [16] comparing experimental data with an analytical transmission model taking into account skull absorption:

$$\alpha_{\text{skull}} = 83\text{Np.m}^{-1}.\text{MHz}^{-1} = 0.72\text{dB.mm}^{-1}.\text{MHz}^{-1} \tag{3}$$

2.1.2. Skull geometric modeling The skull inner and outer surfaces are extracted from the CT scan and modeled with splines. We decided to use a method called Multi-level B-spline Approximation (MBA) [17], which allows a smooth and robust description of the surfaces, but any type of splines can be used. The advantage of MBA over B-Splines is that the user does not have to make a trade-off between the shape smoothness and the accuracy of the interpolation function generated. The resulting function simultaneously achieves a smooth shape while closely approximating the given data. The idea behind MBA is to approximate complex datasets with a hierarchical structure of B-Spline curves. Instead of representing the entire dataset with a single high-degree B-Spline, MBA decomposes the data into multiple lower-degree B-Splines, organized in a hierarchical manner. The lower-degree B-Splines capture the coarse features of the data, while higher-degree B-Splines are used to refine the approximation and capture finer details. A C++ implementation of the MBA algorithm found on GitHub is used (`https://github.com/SINTEF-Geometry/MBA`). This algorithm includes:

- The function to build an MBA surface from a set of 3D points.
- The function $z = f(x, y)$ of the parametric surface.
- The first and second order derivatives of f.

In the general case of splines, each surface is described by a function $f(u, v) = (x, y, z)$. In the case of MBA, $(u, v) = (x, y)$.

To build MBA of the skull inner and outer surfaces from a CT scan, the following steps are performed:

- Extract the skull surface as a STL file (figure 1.(a)) from the DICOM file, with a software such as VG-Studio, ITK-Snap or 3D-Slicer. This is only done once for all transducer positions.
- Cut the skull mesh part located below the transducer using a clip filter with Paraview or MeshLab (figure 1.(a) → figure 1.(b)).
- Convert the cut STL mesh to a MSH mesh using Gmsh (to be used for ray-tracing to find the first guess of the path computation in the next section).

- Extract the inner and outer surfaces of the skull from the cut mesh using a C++ code based on the orientation of the face normal vectors (figure 1.(b) → figure 1.(c)).
- Build the MBA surfaces from the inner and outer mesh vertices (figure 1.(c) → figure 1.(d)).

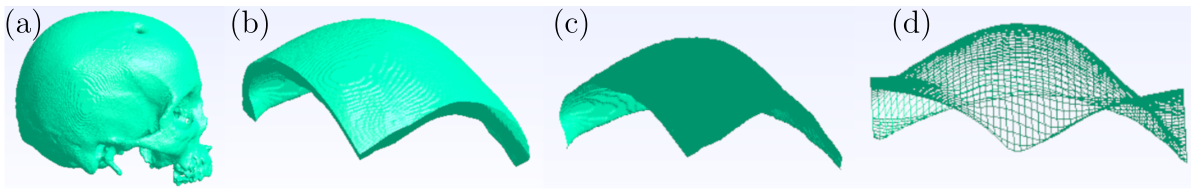

Figure 1: Steps for MBA construction: (a) skull mesh, (b) cut skull mesh, (c) inner cut skull mesh, (d) inner MBA surface.

2.2. Transcranial ultrasound simulation method

The field computation method is similar to a ray-tracing method, but instead of tracing rays, the ultrasonic paths are found by time of flight minimization. 5 paths (1 central and 4 corners) are found for each transducer sample, simulating a ray tube traveling from the sample to a computation point (as in the pencil method [9]). An impulse response can then be computed for each transducer sample. All impulse responses are then summed, and this sum is convoluted with the input signal. The whole field computation algorithm is illustrated is figure 10.

2.2.1. Path computation by time of flight minimization According to Fermat's principle, the ultrasound waves will propagate along the path that can be traveled in the least time. Thus, given a source point and a computation point, the ultrasonic path can be found by minimizing the time-of-flight function. In the case of a homogeneous skull model, illustrated by figure 2, there are only two interfaces 0/1 and 1/2 separating three isotropic homogeneous media of slownesses s_0, s_1 and s_2. Thus, finding the ultrasonic path between a source point P_s and a computation point P_c, comes down to finding the intersection points $I_{0/1}$ and $I_{1/2}$ on the two interfaces, that minimize the time of flight function:

$$\begin{cases} \min_{\mathrm{I}_{0/1},\mathrm{I}_{1/2}} t(I_{0/1}, I_{1/2}) \\ t(I_{0/1}, I_{1/2}) = ||P_s - I_{0/1}||s_0 + ||I_{0/1} - I_{1/2}||s_1 + ||I_{1/2} - P_c||s_2 \end{cases} \tag{4}$$

As the skull is modeled with splines, the two interface surfaces can be described by a function $f(u, v) = (x, y, z)$. Using these functions, the optimization problem can be rewritten as:

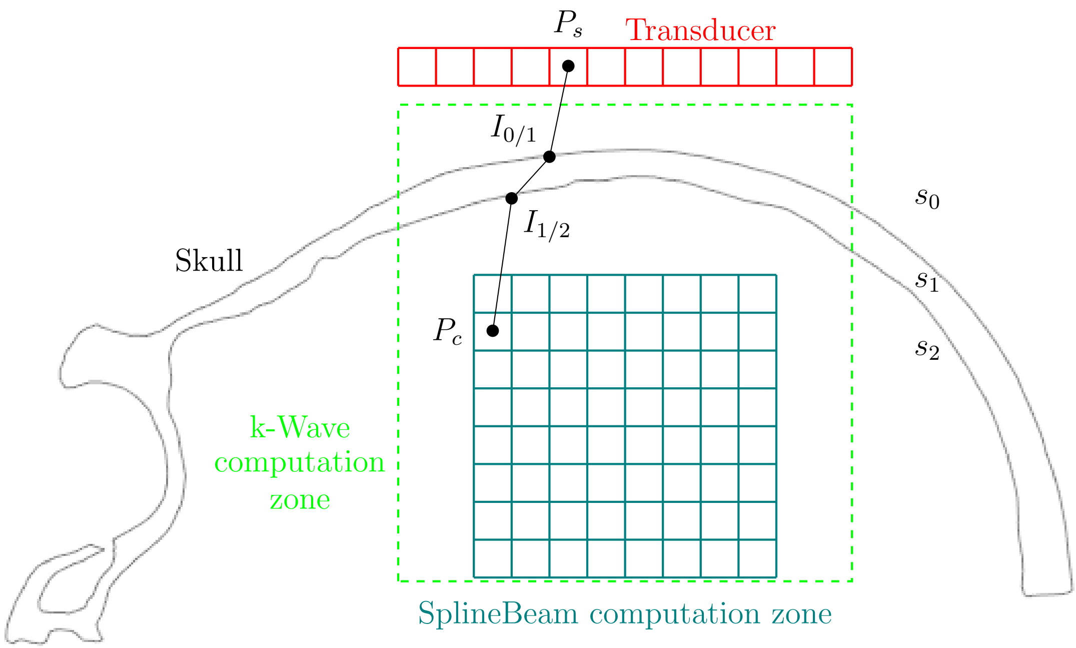

Figure 2: Path computation through a skull.

$$\begin{cases} \min_{(\mathrm{u,v}),(\mathrm{w,x})} t((u,v),(w,x)) \\ t((u,v),(w,x)) = ||P_s - f_{0/1}(u,v)||s_0 + ||f_{0/1}(u,v) - f_{1/2}(w,x)||s_1 + ||f_{1/2}(w,x) - P_c||s_2 \end{cases} \tag{5}$$

As the functions $f_{0/1}$ and $f_{1/2}$ are differentiable, the objective function t is differentiable. The gradient of the objective function is given by:

$$\nabla t = \begin{bmatrix} \frac{\partial t}{\partial u} \\ \frac{\partial t}{\partial v} \\ \frac{\partial t}{\partial w} \\ \frac{\partial t}{\partial x} \end{bmatrix} = \begin{bmatrix} s_0 \frac{\frac{\partial f_{0/1}}{\partial u}.(P_s - f_{0/1}(u,v))}{||P_s - f_{0/1}(u,v)||} + s_1 \frac{\frac{\partial f_{0/1}}{\partial u}.(f_{0/1}(u,v) - f_{1/2}(w,x))}{||f_{0/1}(u,v) - f_{1/2}(w,x)||} \\ s_0 \frac{\frac{\partial f_{0/1}}{\partial v}.(P_s - f_{0/1}(u,v))}{||P_s - f_{0/1}(u,v)||} + s_1 \frac{\frac{\partial f_{0/1}}{\partial v}.(f_{0/1}(u,v) - f_{1/2}(w,x))}{||f_{0/1}(u,v) - f_{1/2}(w,x)||} \\ s_1 \frac{\frac{\partial f_{1/2}}{\partial w}.(f_{0/1}(u,v) - f_{1/2}(w,x))}{||f_{0/1}(u,v) - f_{1/2}(w,x)||} + s_2 \frac{\frac{\partial f_{1/2}}{\partial w}.(f_{1/2}(w,x) - P_c))}{||f_{1/2}(w,x) - P_c||} \\ s_1 \frac{\frac{\partial f_{1/2}}{\partial x}.(f_{0/1}(u,v) - f_{1/2}(w,x))}{||f_{0/1}(u,v) - f_{1/2}(w,x)||} + s_2 \frac{\frac{\partial f_{1/2}}{\partial x}.(f_{1/2}(w,x) - P_c)}{||f_{1/2}(w,x) - P_c||} \end{bmatrix} \tag{6}$$

We thus compute the ultrasonic paths through a skull by solving this optimization problem.

To solve this optimization problem, we use Limited-memory Broyden–Fletcher–Goldfarb–Shanno (L-BFGS) algorithm [18]. A C++ implementation of L-BFGS found on GitHub was used (`https://github.com/twesterhout/lbfgs-cpp`). The minimization algorithm takes as input an evaluation function that gives the value of the objective function and the gradient, parameters for the stopping criteria and a first guess.

As a first guess, we provide L-BFGS the intersection points of the straight path between the source point and the computation point. To obtain these intersection points, we cast a ray from the computation point in the direction of the transducer point using Embree C++ library. The ray is cast on the triangular meshes of the inner and outer surfaces of the skull. The ray casting function gives us, for each one of the two meshes, the intersected triangle and the local 2D coordinates $(u_{\text{local}}, v_{\text{local}})$ of the hit. This data is used to compute the global 2D coordinates $(u_{\text{global}}, v_{\text{global}})$ of the hit by interpolation using:

$$(u_{\text{global}}, v_{\text{global}}) = (1. - u_{\text{local}} - v_{\text{local}})v_0 + u_{\text{local}}v_1 + v_{\text{local}}v_2; \tag{7}$$

where (v_0, v_1, v_2) are the 2D coordinates of the intersected triangle vertices.

The pair of 2D coordinates $(u_{\text{global}}, v_{\text{global}}, w_{\text{global}}, x_{\text{global}})$ is the initial guess given to L-BFGS.

2.2.2. Field computation method The field computation method is based on the pencil method [9], but rather than casting rays from the computation point, the probe is sampled and the path between each probe sample and the computation point is computed by time-of-flight minimization. In both cases, the temporal contributions of all the paths are summed to obtain the impulse response of the ultrasonic field. The advantage of the developed method is that it allows a regular sampling of the probe, as it is defined in advance.

The pencil method, which is the method used in CIVA, was first introduced by Gengembre and Lhémery [19]. In this method, the wavefront is cut into pencils. A pencil is a collection of rays travelling from a source point and diverging slightly. It is composed of an axial ray, following the geometrical path, and the paraxial rays, belonging to the envelope of the pencil. The pencil method allows to compute the divergence factor DF, by computing the cross-section dS of the pencil as a function of the initial solid angle $d\Omega$. The propagation of the pencils is done by computing propagation and interaction matrices for every material and interface encountered by the pencils. The propagation of a pencil is illustrated on the left part of figure 3. The pencil method was later adapted by Chouh et al. [20] for performance purposes, to avoid computing the propagation and interaction matrices. Instead, the paraxial rays of every pencil are cast, using Intel Embree ray-tracing library, so as to reconstitute their contribution. The axial ray and paraxial rays of a pencil are illustrated on the right part of figure 3.

We adapted the pencil method to our path computation method. The principle is very similar to the one proposed by Chouh et al. [20], but instead of casting rays to compute the paths, they are found by time of flight minimization. The advantage of computing the ultrasonic paths by time-of-flight minimization over using ray-tracing, is that each path is defined between a given source point, on the transducer, and the current computation point. Thus, the transducer can be sampled into small squared surfaces, and we can compute a pencil and an impulse response for each sample.

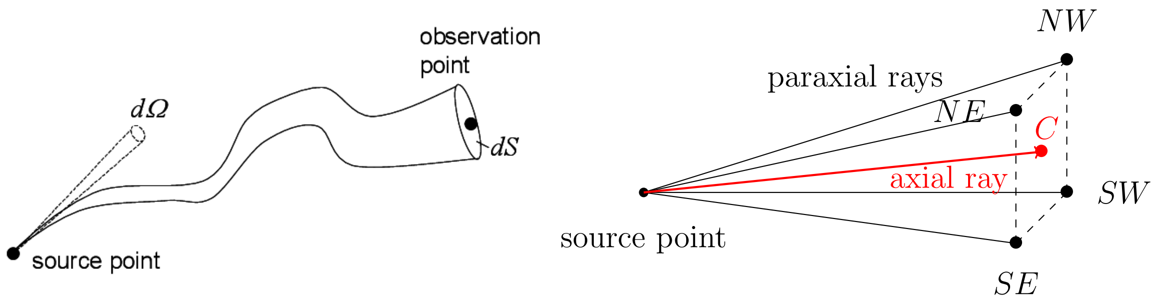

Figure 3: Propagation of a pencil from [21] (right), a pencil with its axial ray and paraxial rays from [20] (left).

The probe, which can be of any geometry, is sampled using a CIVA code that provides the coordinates of the center C, the area dS and the normal n of each sample. The coordinates of the corners of a sample are computed by approximating the sample by a square of center C, area dS and normal n. For each sample, five paths are computed: one from the center (axial ray in the pencil method), four from the corners (paraxial rays in the pencil method). For each sample, these five paths are computed by minimizing the time of flight (as detailed in the previous section) between the sample point and the computation point. They yield: the minimum $t_{\min}$ and maximum $t_{\max}$ times of flight of the sample, the directions of the paraxial rays and the total Fresnel coefficient [22] T_A of the central ray. The paraxial ray directions are used to compute the beam divergence DF [20]. For an input amplitude A_0, the impulse response associated with the surface sample dS is a rectangular signal of amplitude:

$$A_{\mathrm{IR}} = \frac{A_0 \times DF \times T_A \times dS}{t_{\max} - t_{\min}} \tag{8}$$

between $t_{\min}$ and $t_{\max}$. The impulse responses of all probe samples are then summed, and this sum is convoluted with the input signal. The field computation can be broadband or harmonic and can take into account propagation media with a frequency dependent attenuation. We called this field computation algorithm SplineBeam. It is a C++ code, and as the computations are independent for all computation points, we parallelized it with Intel library Threading Building Blocks (TBB).

2.3. Experimental validation

We measured pressure fields through an *ex vivo* human skull sample with a hydrophone to experimentally validate SplineBeam. Then we compared those pressure fields with the ones simulated with SplineBeam as well as other methods (k-Wave and CIVA).

The skull sample used in the experiments is a half human skull, cut in the sagittal plane. It was provided by Grenoble-Alpes CHU anatomic pathology laboratory. The skull is attached to an aluminum positioning frame with nylon screws (to avoid artefacts on the CT scan). The positioning frame has four landmarks used to locate the skull coordinate system. The skull (initially preserved dry), together with the positioning frame, is immersed in water and degassed for at least 48h to mimic *in vivo* conditions. To obtain the skull shape and acoustic properties as explained in chapter 2.1, two CT scans of the skull were performed. The first one was made with the skull attached to its positioning frame to have a precise positioning in the simulations. The problem with this scan, is that it contained too many artefacts because of the aluminium positioning frame. Thus, after all experiments were done, another CT scan was performed with the skull alone (degassed in water), to obtain a cleaner scan to be able to obtain the skull geometry and acoustic properties. The meshes extracted from the two scans were registered with the "align tool" of MeshLab. Both scans were performed with a SIEMENS Biograph Horizon scanner at Service Hospitalier Frédéric Joliot (Orsay, France). The CT scan parameters are given in table 2.

Table 2: CT scan parameters.

Voxel spacing	Slice thickness	Reconstruction kernel	Peak voltage
$0.59 \times 0.59 \times 0.50\text{mm}^3$	0.75mm	J80s	130kVp

The transducer emits pulses of 10μs at a frequency of 0.4MHz. The transducer is spherically curved, has a radius of 55mm and a natural focal length of 110.65 mm, which is close to the skull curvature radius to allow maximum ultrasound transmission. The transducer is composed of 16 annular elements, which, with delay laws, can be used to focus at different depths behind the skull. In our case, no delay laws were used. A UR5 robot arm and a 3D printed support were used to precisely position the transducer relative to the skull. Indeed, the robot can be calibrated to register the skull coordinate system and then execute precise trajectories (with a repeatability of $\pm$0.1mm) in that coordinate system.

Three transducer positions, relative to the skull, were chosen so that the ultrasound crosses different parts of the skull for the three positions. All three positions do not target the same point. The three transducer positions are displayed in figure 4. For these three configurations, the transducer is around 30mm away from the skull outer surface.

The hydrophone Onda HGL-0400 (Golden lipstick, aperture size 400 μm) is combined with a preamplifier Onda AG-2010 and a Picoscope 5000A. The picoscope is connected to the computer, and a Python script was coded to register the measured signals. The hydrophone and preamplifier are attached, thanks to a 3D printed support, to a 3D positioning system that can move in the directions (x,y,z). A Python script was coded to automate the scan.

As explained before, the skull coordinate system can be registered using the robot. The coordinates of the four landmark points (on the skull positioning frame) in the skull coordinate system are given to the robot software. Then, the position of the landmarks

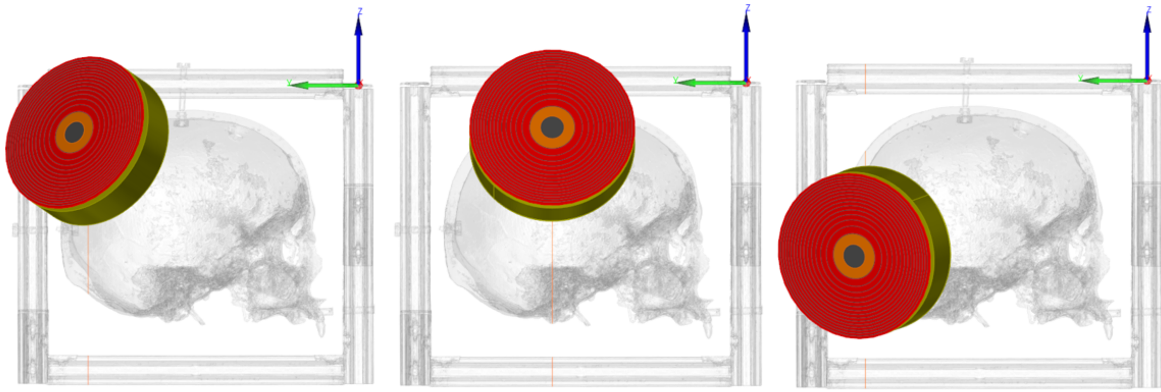

Figure 4: The 3 transducer positions displayed in CIVA.

in the robot coordinate system are recorded. To do so, a spike (of very well-known geometry) is attached to the robot, and the latter is move manually so that the spike hits each one of the four landmarks, as shown on the left hand side of figure 5. The robot software is then able to localize the robot in the skull coordinate system.

To precisely put the computation zone in the simulations at the same position as the hydrophone, one needs to find the change of basis matrix between the hydrophone coordinate system and the skull system. To do so, four points are chosen in the hydrophone coordinate system and the robot is moved manually so that the spike hits each one of those points, as shown on the right hand side of figure 5. When a point is hit with the spike, the robot software displays the corresponding coordinate in the skull system. In order not to damage the hydrophone tip, a printed copy of the hydrophone, with the same dimensions as the real one, was used instead. This can add some error due to small changes between the two mechanical pieces and repeatability of the exact positioning of the real hydrophone compared to the hydrophone printed copy.

This precise protocol enabled us to achieve a positioning error between 1.12mm and 1.25mm. Indeed, after each scan through the skull, the skull was removed and a scan without skull (with the hydrophone and transducer kept at the same positions) was performed. The positioning error was then computed as the difference in focal position between the experiments and the simulations, once the skull is removed. Once all the elements are in place, a 3D pressure scan is performed by the hydrophone attached to the 3D positioning system, which is itself driven by a Python code. The signals recorded at each point are then post-processed, also using a Python code. For each signal, a finite impulse response filter is applied to clean the data, then the Hilbert transform is applied to get the envelope of the absolute value of the signal. Finally, the maximum of the envelope is saved in a 3D matrix containing the whole scan.

The protocol was first validated using measurements without the skull as a reference. Then, three transcranial fields were measured for three probe positions, illustrated in figure 6.

Finally, we compared those pressure fields with the ones simulated with SplineBeam

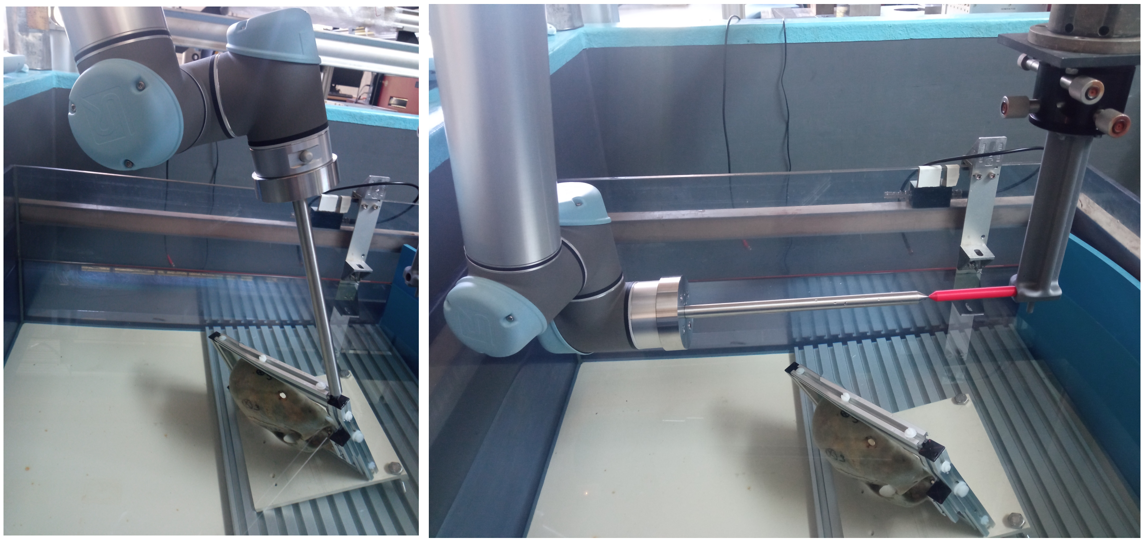

Figure 5: Calibration steps: skull coordinate system registration (left), hydrophone printed copy coordinate system registration (right).

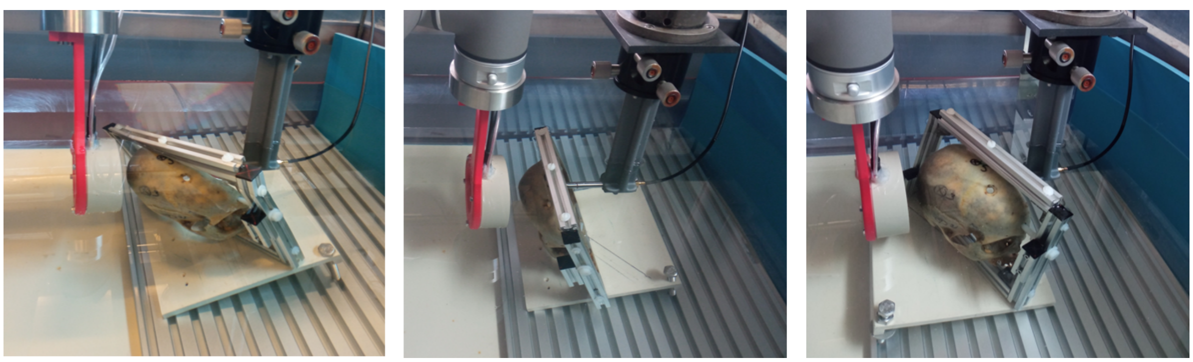

Figure 6: The 3 experimental transducer positions.

as well as other methods (k-Wave and CIVA), using the following metrics:

2.3.1. Focal spot position error The focal spot position error ΔX_{max} is computed after artificially correcting the positioning error. The positioning error was artificially corrected by translating the transducer in the simulations so that the difference in focal position between the simulated and measured fields without skull is null. The focal spot position error ΔX_{max} is then computed in mm as:

$$\Delta X_{max} = ||X_{max}^{skull,exp} - X_{max}^{skull,simu}|| \tag{9}$$

where $X_{max}^{skull,exp}$ and $X_{max}^{skull,simu}$ are the maximum pressure positions of the experimental and simulated fields for the configurations with skull.

2.3.2. Maximum pressure error The maximum pressure error or focus amplitude error ΔP_{max} is computed in % as:

$$\Delta P_{max} = \frac{\left| P_{max}^{skull,exp} / P_{max}^{water,exp} - P_{max}^{skull,simu} / P_{max}^{water,simu} \right|}{P_{max}^{skull,exp} / P_{max}^{water,exp}} \tag{10}$$

where $P_{max}^{skull,exp}$ and $P_{max}^{skull,simu}$ are the maximum pressure values (over the whole field) of the experimental and simulated fields for the configurations with skull, and $P_{max}^{water,exp}$ and $P_{max}^{water,simu}$ are the maximum pressure values of the experimental and simulated fields for the configurations with skull but with the skull removed. Indeed, all simulated and measured fields were normalized with respect to the corresponding fields without skull.

2.3.3. Focal volume error The focal volume error ΔV_{focal} is computed as:

$$\Delta V_{focal} = \frac{|V_{focal}^{skull,exp} - V_{focal}^{skull,simu}|}{V_{focal}^{skull,exp}} \tag{11}$$

where $V_{focal}^{exp,skull}$ and $V_{focal}^{simu,skull}$ are the -3dB volumes (or focal spot volume) of the experimental and simulated fields for the configurations with skull.

2.3.4. L^2 error Finally, the L^2 relative norm between an experimental field and a simulated field was computed as:

$$L^2 = \sqrt{\frac{\sum \left(P_i^{skull,exp} / P_i^{water,exp} - P_i^{skull,simu} / P_i^{water,simu} \right)^2}{\sum \left(P_i^{skull,exp} / P_i^{water,exp} \right)^2}} \tag{12}$$

where $P_i^{skull,exp}$ and $P_i^{skull,simu}$ are the pressure values at each point i of the experimental and simulated fields for the configurations with skull, and $P_i^{water,exp}$ and $P_i^{water,simu}$ are the pressure values at each point i for the configurations with skull but with the skull removed.

2.3.5. K-Wave simulations The k-Wave simulations were run using a CIVA plug-in we created, that allows to run a k-Wave simulation from CIVA interface. The configuration is defined in CIVA, which allows to create the transducer geometry from CIVA interface. Then, the pressure field in a plane parallel to the transducer (the input plane of the computation zone) is computed with CIVA. The resulting pressure field in this plane is used as input to run the "kspaceFirstOrder3D" solver (Matlab code to be able to take attenuation into account) over the whole computation zone. The resulting field can then be read with CIVA interface. This plug-in allows to define the transducer geometry with CIVA, and thus to have the same transducer geometry as in SplineBeam and CIVA simulations.

The k-Wave simulations were run using a spatial resolution of 7.5 points per wavelength (a convergence test was performed to choose this spatial step) and temporal resolution of 50 points per period (thus with a CFL number of 0.15). The simulated time period was $70\mu s$ and the computations were broadband.

All simulations (SplineBeam, CIVA and k-Wave) were run on a laptop (2.3GHz, 8 cores).

3. Results

3.1. Numerical validation

SplineBeam was first numerically validated by comparison with other methods from the literature, thanks to the very useful benchmark study by Aubry et al. [23]. This study compares 11 solvers (including k-Wave) on 9 benchmark configurations with 2 different transducers: a focused bowl (sc1) and a plane piston (sc2). Both transducers operate at 500kHz. The configurations contain layers of bone of increasing geometric complexity.

SplineBeam was run on all benchmark configurations, except on the ones with more than 3 media, that is to say the ones including a layer of skin or trabecular bone: benchmark n°4 and 6. Indeed, SplineBeam is so far unable to compute a pressure field through more than two surfaces and thus through more than three media. In addition, as SplineBeam can so far only compute the field in the third medium, the computation zones were reduced to the focal spot.

For all benchmark configurations on which SplineBeam was run, the focus position difference $\Delta X_{\max}$ and maximum amplitude difference $\Delta P_{\max}$ relative to k-Wave are displayed in table 3. k-Wave was chosen for the comparison, as it is considered as the reference in this study. The comparison of all solvers with SplineBeam is shown on figures 11 and 12 displayed in the appendix.

The comparison of SplineBeam with other solvers (table 3) shows a good agreement. The focus position difference between SplineBeam and k-Wave is always less than 1.50mm and the maximum pressure difference is always less than 8%.

For the 4 configurations in water, both metrics are very low ($\Delta X_{\max} \leq 0.5$mm and $\Delta P_{\max} \leq 1.31\%$), which shows that SplineBeam simulates well the ultrasound propagation in very simple media. There is only a focus position difference of 0.5mm for configuration BM2-SC1, which is equal to the spatial step of the computation zone used for SplineBeam. The error could be due to the difference of geometry of the source n°1, which is analytic with SplineBeam and grid projected with k-Wave.

For the 4 configurations through bone with analytical shapes (flat and sphere), the focus position differences are quite low ($\Delta X_{\max} \leq 1$mm) whereas the maximal pressure differences are a bit higher ($\Delta P_{\max} \leq 7.29\%$), especially for BM3-SC1 and BM5-SC1. We thought this difference in amplitude was due to the fact that SplineBeam neglects internal reflections, whose influence can be important for such regular geometries. Thus, we ran CIVA simulations with and without reflections and compared them with SplineBeam and k-Wave. For configurations BM3-SC1 and BM5-SC1, the maximum pressure of CIVA-with-reflections fields and k-Wave fields were very close ($< 0.8\%$),

Table 3: SplineBeam errors relative to k-Wave on the benchmark configurations proposed by Aubry et al. [23].

Configuration	Material	Shape	$\Delta X_{\max}$ (mm)	$\Delta P_{\max}$ (%)
BM1-SC1	Water	None	0.00	0.07
BM1-SC2	Water	None	0.00	1.31
BM2-SC1	Water[a]	None	0.50	0.03
BM2-SC2	Water[a]	None	0.00	0.42
BM3-SC1	Bone	Flat	0.00	4.21
BM3-SC2	Bone	Flat	0.00	0.27
BM5-SC1	Bone	Sphere	1.00	7.29
BM5-SC2	Bone	Sphere	0.50	2.58
BM7-SC1	Bone	Skull	0.00	4.46
BM7-SC2	Bone	Skull	0.50	5.11
BM8-SC1	Bone[b]	Skull	1.50	2.80
BM8-SC2	Bone[b]	Skull	1.00	4.25
BM9-SC1	Bone[b]	Skull	1.00	1.37
BM9-SC2	Bone[b]	Skull	1.12	3.43

[a] Water with attenuation.
[b] With brain inside the skull.

and the maximum pressure of CIVA-without-reflections fields and SplineBeam fields were very close ($< 1.1\%$). This confirms that, at least part of the maximum pressure difference between SplineBeam and k-Wave is due to the fact that SplineBeam does not take reflections into account.

For the 6 configurations through skulls, the differences in focus position are a bit higher than for the previous configurations but still reasonable ($\Delta X_{\max} \leq 1.5$mm). The differences in focus amplitude are a bit lower than for the analytical configurations ($\Delta P_{\max} \leq 5.11\%$), which shows that the influence of internal reflections is decreased for more complex geometries. These comparisons show that SplineBeam is able to simulate correctly the ultrasound propagation through skull samples. We believe the small differences are probably due to the skull geometry modeling which is very different between k-Wave and SplineBeam. We think that the spline model is closer to the skull real shape than the stair-like geometry imposed by k-Wave grid which depends on the grid step.

3.2. Experimental validation

The measured and SplineBeam simulated pressure field planes for all 3 transducer positions are displayed in figures 7, 8 and 9. The difference between the simulated and experimental fields is also plotted for better analysis. All fields are in percentage of the maximum pressure of the fields without skull (the simulated pressure fields with skull are normalized with respect to the simulated pressure fields without skull and the experimental pressure fields with skull are normalized with respect to the experimental pressure fields without skull).

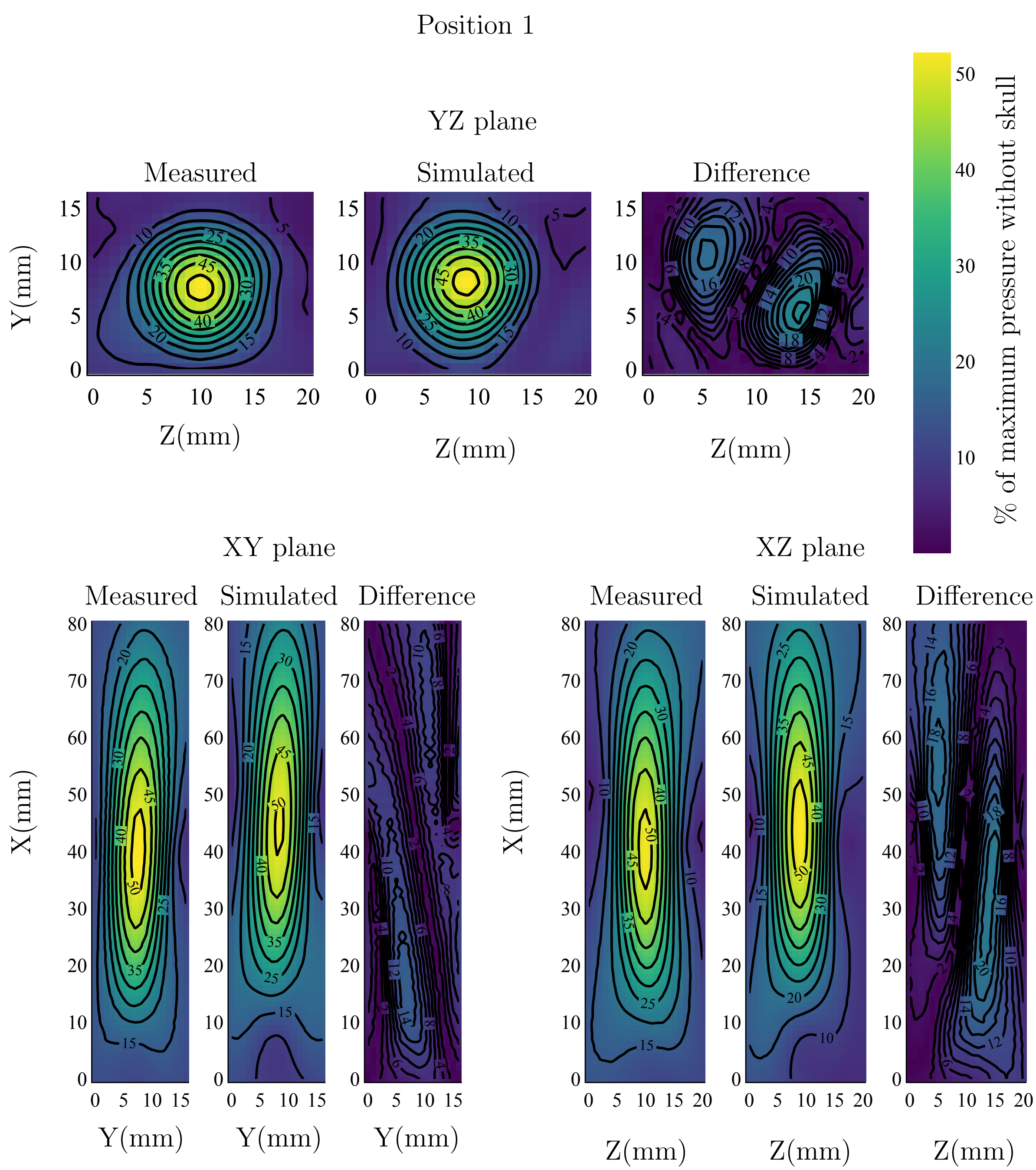

Figure 7: Experimental and simulated pressure field planes for transducer position n°1.

These figures show that, qualitatively, SplineBeam simulated pressure fields are close to the measured ones, for all transducer positions.

For all 3 transducer positions, the focus position error $\Delta X_{\max}$, the focus amplitude error $\Delta P_{\max}$, the focal volume error ΔV_{focal} and the L^2 error between the experimental

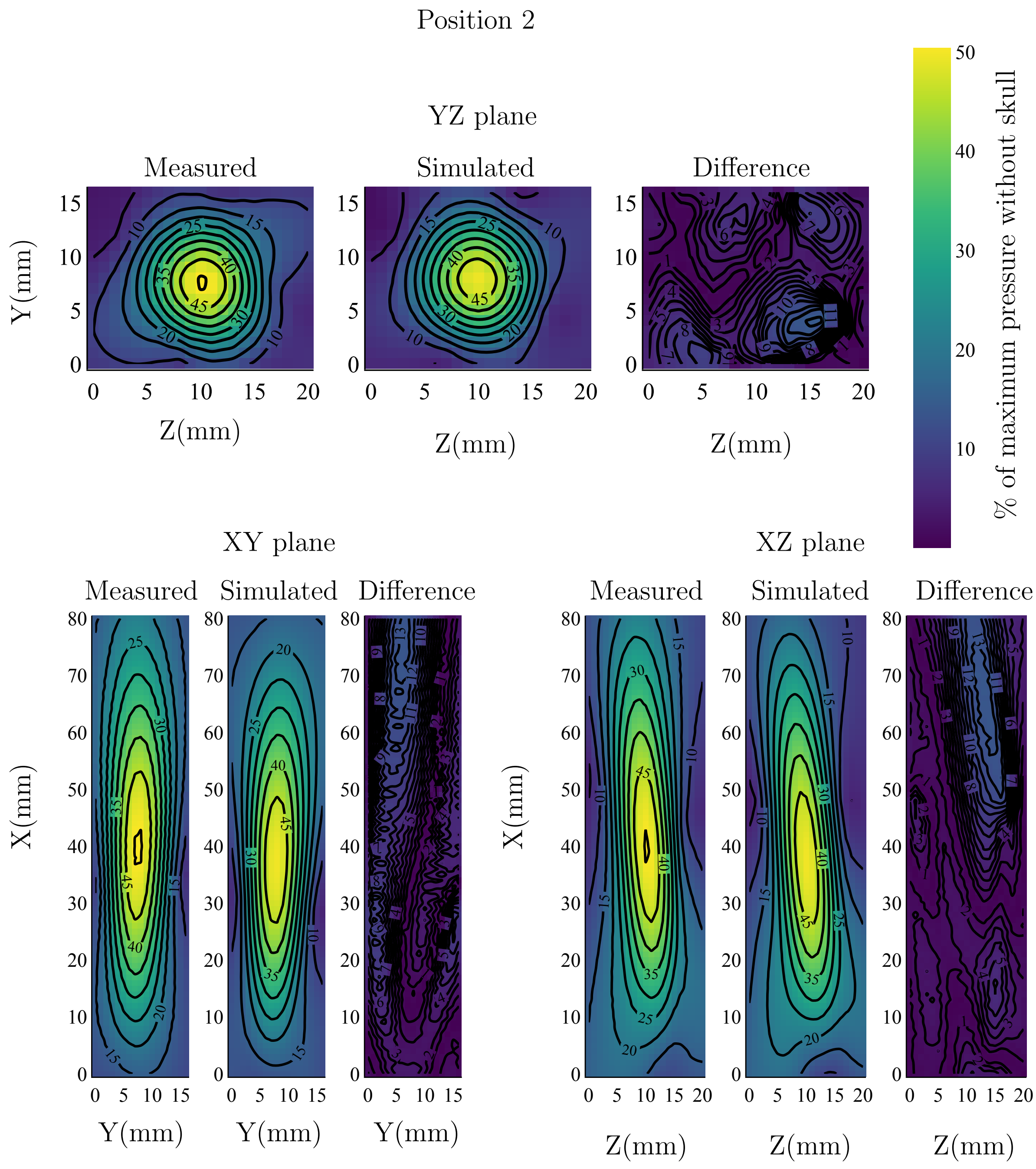

Figure 8: Experimental and simulated pressure field planes for transducer position n°2.

and simulated (either with SplineBeam, CIVA or k-Wave) fields are displayed in table 4. k-Wave is run with a homogeneous skull model and a heterogeneous one.

Table 4 shows overall a good agreement between the measured pressure fields and the simulated ones with all simulation methods. Most focus position errors are between 1mm and 2mm. Most maximum pressure errors are lower than 26% in absolute value, which is very low compared to the difference of maximum pressure between the

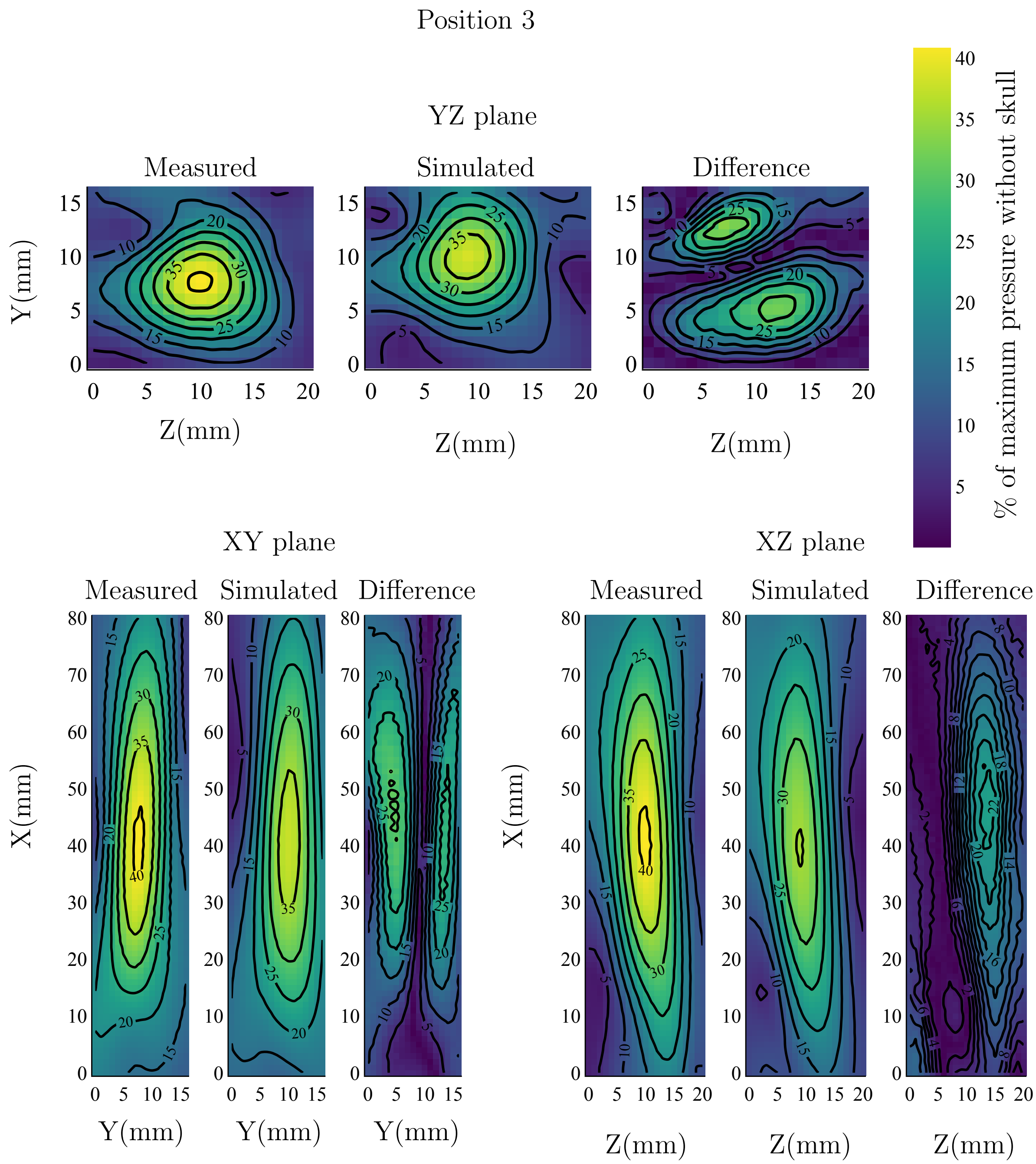

Figure 9: Experimental and simulated pressure field planes for transducer position n°3.

measurements with and without skull (which is always around 50%). The focal volume errors are all lower than 20%, which corresponds approximately to a one dimensional error of 7%, which is reasonable. In addition, the focal volume errors sometimes reached 15% for configurations without skull, which shows that the focal volume errors for the configurations with skull are not that high. Finally, the L^2 norm between the experimental and simulated fields is always under 33%, which is not that high given

Table 4: Comparison of the simulated pressure fields with the experimental ones for the configurations through the skull sample.

Position	Comparison	$\Delta X_{\max}$	$\Delta P_{\max}$	ΔV_{focal}	L^2
1	SplineBeam/Exp	1.58mm	−1.64%	0.28%	23.13%
	k-Wave heterogeneous/Exp	1.58mm	−25.86%	6.16%	26.58%
	k-Wave homogeneous/Exp	2.55mm	−19.88%	1.75%	26.65%
	CIVA/Exp	2.06mm	+1.60%	3.74%	24.14%
2	SplineBeam/Exp	1.00mm	+1.89%	11.70%	12.82%
	k-Wave heterogeneous/Exp	1.12mm	−25.64%	18.26%	20.56%
	k-Wave homogeneous/Exp	1.50mm	−18.97%	16.20%	17.47%
	CIVA/Exp	1.50mm	+22.22%	11.88%	32.25%
3	SplineBeam/Exp	1.12mm	+6.02%	14.82%	29.63%
	k-Wave heterogeneous/Exp	2.60mm	−1.34%	15.38%	17.09%
	k-Wave homogeneous/Exp	1.87mm	−14.47%	11.97%	30.85%
	CIVA/Exp	1.22mm	+4.78%	6.77%	29.23%

that focus position errors are all above 1mm.

The maximum pressure position error is lower for SplineBeam than for the other simulation methods for all 3 positions. It is always under 1.6mm, but never drops below 1mm, which was expected given that the measurement positioning errors are around 1mm and that the focal position errors for configurations without skull sometimes reached 1mm. k-Wave with a heterogeneous skull model also gives small maximum pressure position errors (< 1.6mm), except for position 3, where the error is even bigger than the difference with/without skull by 0.5mm.

The maximum pressure error for SplineBeam is very low ($< 7\%$ in absolute value) for all 3 configurations. It is possibly biased by the choice of the attenuation coefficient which is widely debated in the literature. However, the values of $\Delta P_{\max}$ are closer to each other than with k-Wave heterogeneous or with CIVA, which suggests that for k-Wave heterogeneous and CIVA there does not exist any value of attenuation coefficient such that all $\Delta P_{\max}$ are low. With k-Wave homogeneous, the values of $\Delta P_{\max}$ are also close to each other, which suggests that with another attenuation coefficient value, this simulation method could give realistic results in terms of maximum pressure.

In terms of focal volume, CIVA gives overall the lowest errors (in average 7.46%), while k-Wave heterogeneous gives the highest ones (in average 13.27%).

The lowest L^2 errors are obtained with k-Wave heterogeneous and SplineBeam with averaged values of respectively 21.41% and 21.86% for the three transducer positions, while the two other simulation methods give average L^2 errors higher than 25%

Overall, SplineBeam has quite low errors and lower than the other simulation methods.

When comparing k-Wave simulations with a homogeneous skull model versus with a heterogeneous skull model, we notice that the homogeneous skull model gives better results in terms of focal volume for the 3 configurations, by in average 3%. For the first two positions, the homogeneous model gives better results in terms of maximum pressure value (by in average 6.33%) while the heterogeneous one gives better results in terms of maximum pressure position (by in average 0.67mm), except for transducer position 3 for which it is the opposite: the heterogeneous model gives better results in terms of maximum pressure value (by 13.13%) while the homogeneous one gives better results in terms of maximum pressure position (by 0.73mm). Taking these three metrics into account, the heterogeneous and homogeneous models are approximately equivalent. In terms of L^2 error, the heterogeneous model is slightly better than the homogeneous one (by less than 4%). This shows that the homogeneous and heterogeneous models are approximately equivalent in terms of focal metrics, but that the heterogeneous model is able to simulate more details of the pressure field. This observation provides a first experimental validation of the homogenization method developed in our previous study [13].

3.3. Computation time

We compared SplineBeam and k-Wave computation time for broadband BM7-SC1 with and without attenuation and for a same number of computation points for various number of threads on a laptop on a laptop (2.3GHz, 8 cores). The computation times are displayed in table 5.

Table 5: Comparison of SplineBeam and k-Wave computation time for broadband BM7-SC1 with and without attenuation and for a same number of computation points for various number of threads.

Simulation	SplineBeam		k-Wave	
Attenuation	With	Without	With	Without
1 thread	1573s	1530s	239s	106s
4 threads	720s	660s	54s	54s
8 threads	120s	120s	41s	18s

With 8 threads, table 5 shows that k-Wave was in average 7 times faster than SplineBeam for computations without attenuation (k-Wave C++ code) and 3 times faster than SplineBeam for computations with attenuation (k-Wave Matlab code). However, this is for a same number of computation points, and SplineBeam has many advantages that allows it to reduce the number of computation points. First, unlike k-Wave, there is no convergence condition on SplineBeam spatial step, thus the computation zone step can be increased. Taking a spatial step two times larger in the 3 directions would result in a reduction by 8 of the computation time. Second, SplineBeam computation zone can be reduced to the focal spot, allowing to reduce the computation time a lot depending on the configuration. Finally, for computations with attenuation, k-Wave Matlab code is not well parallelized, which means that SplineBeam would probably be faster on a computer with more than 8 cores, for a same number of computation points.

To show the potential of computing the field only at the focal spot, let us study the computation times of the experimental configurations. The computation time for each one of the 3 experimental configurations was around 3 minutes for SplineBeam and 6 hours for k-Wave (the Matlab code was used as frequency dependent attenuation was modeled) on a laptop (2.3GHz, 8 cores). This means that SplineBeam was around 120 times faster than k-Wave. This was mainly due to the fact that k-Wave computation zone was much bigger as it needs to include the skull and the whole transducer width, as shown in figure 2. k-Wave computation zone was approximately 275 times bigger than SplineBeam's. Thus, for a same number of computation points, k-Wave would have had a computation time of around 1.3min, so around 3 times faster than SplineBeam (as written above). However, for these configurations, k-Wave computation zone cannot be smaller, and SplineBeam does not need a bigger computation zone. This shows a practical example where SplineBeam is much faster (by two orders of magnitude) than k-Wave, thank to its capacity to compute the field only at the focal spot.

4. Discussion

A new semi-analytical transcranial ultrasound simulation method based on time of flight minimization, was developed. This method, called SplineBeam, was numerically validated by comparison with other solvers. Then, SplineBeam's ability to compute realistic pressure fields through the skull was verified experimentally. Finally, SplineBeam computation time was evaluated.

The numerical validation showed that SplineBeam simulated pressure fields were close to the ones simulated by other solvers. Indeed, the focus position difference compared to k-Wave was lower than 1.5mm and the maximum pressure difference relative to k-Wave lower than 8%. It showed that SplineBeam is able to correctly simulate transcranial pressure fields. However, only comparisons with a "ground truth" such as hydrophone measurements can show which method provides the most realistic fields. That is why SplineBeam was then experimentally validated by comparing simulated pressure fields with hydrophone measured ones through a human skull sample. SplineBeam simulated pressure fields were very similar to the measured ones, for all focal metrics (position, amplitude and volume), as well as the L^2 norm. It shows that the simulation method developed as well as the skull model are realistic. SplineBeam simulated pressure fields were closer to the measured ones than k-Wave simulated ones. This confirms the potential of semi-analytical methods for transcranial ultrasound simulations. In addition, SplineBeam simulated pressure fields were closer to the measured ones than CIVA simulated ones. This confirms the advantage of the new path computation method and the smooth skull model developed in SplineBeam, over ray-tracing and the mesh model used in CIVA. The measurements also allowed evaluating the homogenization method alone, by comparing the pressure fields computed with k-Wave with a homogeneous skull model and with a heterogeneous one. The pressure fields simulated through both models were approximately equivalent in terms of focal spot metrics. Indeed, the heterogeneous model was in average a bit better than the homogeneous one in terms of focal spot position (by 0.21mm) and of focal pressure (by 0.16%), while the homogeneous was in average a bit better than the heterogeneous one in terms of focal volume (by 3.29%). This shows that a homogeneous description of the skull can be enough, with a homogenization method more realistic than the averaging method. Finally, SplineBeam computation time was evaluated. It is a bit higher than k-Wave for a same number of computation points. However, the advantage of SplineBeam is that, unlike k-Wave, it has no constraints on the spatial step nor the computation zone size, which allows it to reduce drastically the number of computation points, and thus be faster than k-Wave by two orders of magnitude for some practical cases (such as the experimental configurations presented in section 3.2) where the region of interest is much smaller than the ultrasound propagation zone.

Regarding the simulation method developed, the next upgrades would be to generalize the path computation algorithm so that SplineBeam can compute pressure fields through any number of interfaces. It will allow, for transcranial simulations or aberration correction, to include a layer of skin, or to model the skull as a three layer medium (cortical bone - trabecular bone - cortical bone), or even as a multi-layer medium as is done in [24]. In addition, it will allow to compute the field in the first and second layers. Finally, it will allow to include reflections inside the layers. To further validate SplineBeam, more experimental measurements could be carried out. Indeed, more transducer positions could be performed, several skull samples and transducers could be used. Comparing the measured and simulated pressure fields through several skull samples would allow to confirm the value of the attenuation coefficient (specific to our simulation method and skull model), or to determine a more complicated attenuation law. Besides, the positioning error of the measurements is still a bit too high compared to the skull induced focus shift. Thus, the positioning protocol needs to be further improved, for example by using a new material for the skull positioning frame, that could combine rigidity and CT scan compatibility. However, we know it would be hard to have a positioning error below the standard CT scan resolution of around 0.6mm. Finally, the hydrophone measured fields can not be considered as an absolute truth as the hydrophone measurements are not always repeatable. This is probably due to the hydrophone finite precision that we have not quantified here. In terms of computation time, SplineBeam is quite fast (3 minutes on a laptop for the experimental configurations) but still not enough to reach real time computations (that is to say in the order of a few seconds). The main limitation in terms of computation time is the optimization algorithm L-BFGS used to compute the ultrasonic paths. Thus, a GPU version of L-BFGS could be used or a faster optimization algorithm could be used.

5. Conclusion

A new semi-analytical transcranial ultrasound simulation method, called SplineBeam, was developed. SplineBeam is able to simulate realistic transcranial pressure fields, as the focus position difference between the simulated and experimentally measured pressure fields was lower than 1.58mm (and of the order of the positioning error of the measurements) and the maximum pressure difference was lower than 6.02%. In addition, SplineBeam was shown to be fast, as on the experimental configurations, SplineBeam computation time was lower than k-Wave's by two orders of magnitude, thanks to its capacity to compute the field only at the focal spot. Thus, SplineBeam is able to compute fast and realistic transcranial pressure fields. The combination of this two assets makes it a promising tool for real time transcranial pressure field prediction during ultrasound brain therapy interventions.

Acknowledgments

Appendix

Diagram of the computation field algorithm steps:

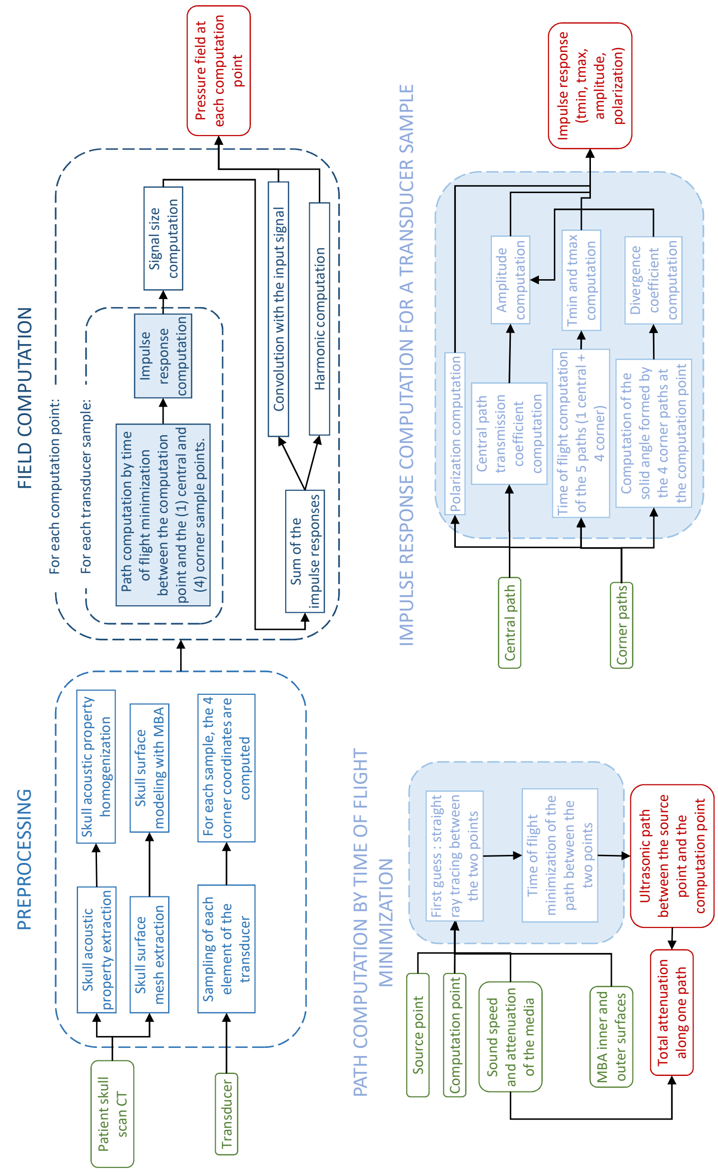

Figure 10: Diagram of the computation field algorithm steps (detailed in section 2)

Boxplots of the focal position error and focal amplitude error of all solvers compared to SplineBeam on the benchmark configurations proposed by Aubry et al. [23].

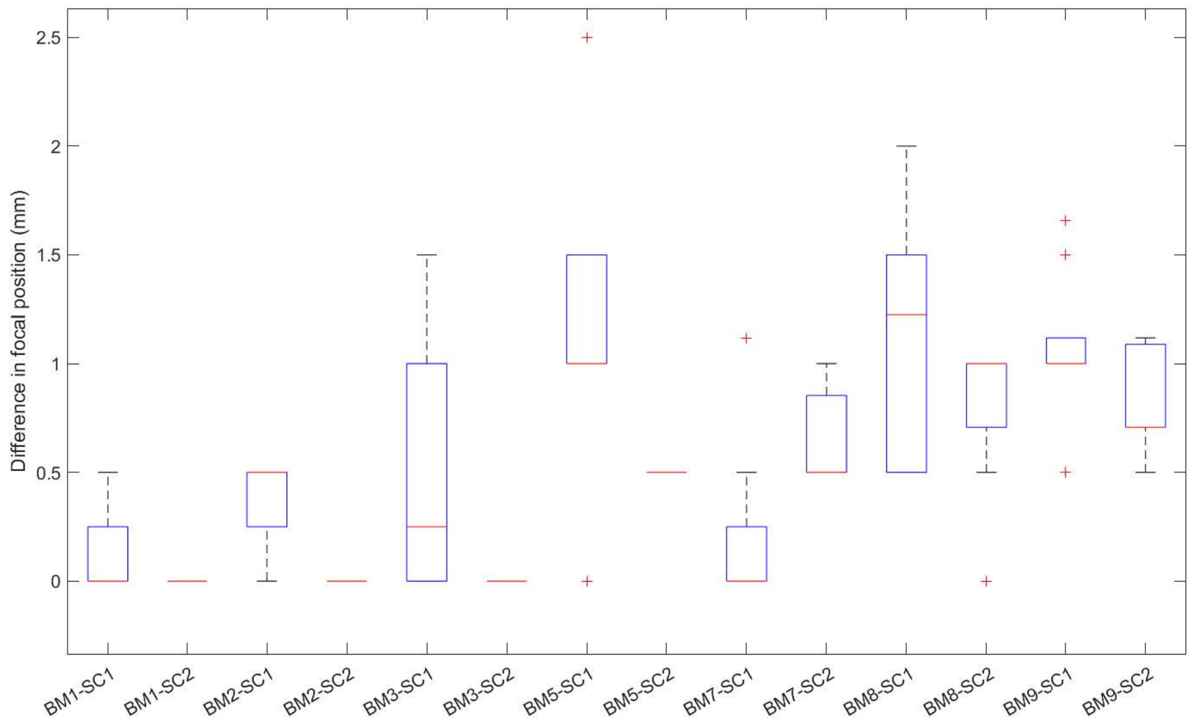

Figure 11: Boxplots of the focal position differences of all solvers relative to SplineBeam on the various benchmark configurations.

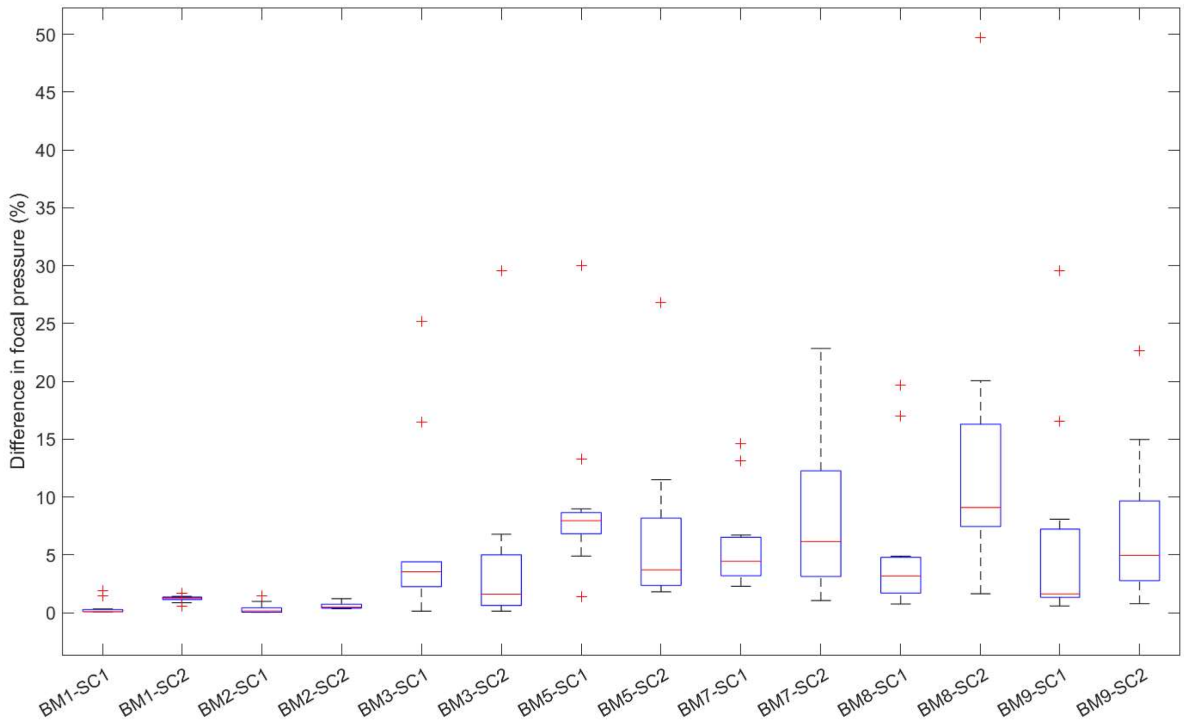

Figure 12: Boxplots of the focal pressure differences of all solvers relative to SplineBeam on the various benchmark configurations.

References

[1] Matthias Reinhard, Andreas Hetzel, Sebastian Krüger, Stefan Kretzer, Jochen Talazko, Sargon Ziyeh, Johannes Weber, and Thomas Els. Blood-brain barrier disruption by low-frequency ultrasound. *Stroke*, 37(6):1546–1548, 2006.

[2] Emily White. *Focused Ultrasound Foundation State of the Field Report 2021*. 2021.

[3] Timothy Wagner, Antoni Valero-Cabre, and Alvaro Pascual-Leone. Noninvasive human brain stimulation. *Annual review of biomedical engineering*, 9:527–565, 2007.

[4] Jean-François Aubry, Mickael Tanter, Mathieu Pernot, Jean-Louis Thomas, and Mathias Fink. Experimental demonstration of noninvasive transskull adaptive focusing based on prior computed tomography scans. *The Journal of the Acoustical Society of America*, 113(1):84–93, 2003.

[5] Yun Jing, F. Can Meral, and Greg T. Clement. Time-reversal transcranial ultrasound beam focusing using a k-space method. *Physics in Medicine and Biology*, 57(4):901–917, 2012.

[6] Bradley E. Treeby, Jakub Budisky, Elliott S. Wise, Jiri Jaros, and B. T. Cox. Rapid calculation of acoustic fields from arbitrary continuous-wave sources. *The Journal of the Acoustical Society of America*, 143(1):529–537, 2018.

[7] Célestine Angla, Benoit Larrat, Jean Luc Gennisson, and Sylvain Chatillon. Transcranial ultrasound simulations: A review. *Medical Physics*, 50(2):1051–1072, 2023.

[8] Chen Jiang, Dan Li, Feng Xu, Ying Li, Chengcheng Liu, and Dean Ta. Numerical Evaluation of the Influence of Skull Heterogeneity on Transcranial Ultrasonic Focusing. *Frontiers in Neuroscience*, 14, 2020.

[9] Robert Andrew Drainville, Sylvain Chatillon, David Moore, John Snell, Frederic Padilla, and Cyril

Lafon. A simulation study on the sensitivity of transcranial ray-tracing ultrasound modeling to skull properties. *The Journal of the Acoustical Society of America*, 154(2):1211–1225, 2023.

[10] Thomas Bancel, Alexandre Houdouin, Philippe Annic, Itay Rachmilevitch, Yeruham Shapira, Mickaël Tanter, and Jean-François Aubry. Comparison between ray-tracing and full-wave simulation for transcranial ultrasound focusing on a clinical system using the transfer matrix formalism. *IEEE Transactions on Ultrasonics, Ferroelectrics, and Frequency Control*, 68(7):2554–2565, 2021.

[11] Adamos Kyriakou, Esra Neufeld, Beat Werner, Gábor Székely, and Niels Kuster. Full-wave acoustic and thermal modeling of transcranial ultrasound propagation and investigation of skull-induced aberration correction techniques: a feasibility study. *Journal of therapeutic ultrasound*, 3(1):11, 2015.

[12] Scott Almquist, Dennis L. Parker, and Douglas A. Christensen. Rapid full-wave phase aberration correction method for transcranial high-intensity focused ultrasound therapies. *Journal of Therapeutic Ultrasound*, 4(1), 2016.

[13] Célestine Angla, Benoit Larrat, Jean Luc Gennisson, and Sylvain Chatillon. Improved skull bone acoustic property homogenization for fast transcranial ultrasound simulations. *Proceedings of the 20th Anglo-French Physical Acoustics Conference, to be published in the J. Phys.: Conf. Ser., submitted.*

[14] Laurent Marsac, Dorian Chauvet, Raphaël La Greca, Ann-Laure Boch, Kathia Chaumoitre, Mickael Tanter, and Jean-Francois Aubry. Ex vivo optimisation of a heterogeneous speed of sound model of the human skull for non-invasive transcranial focused ultrasound at 1 MHz. *International Journal of Hyperthermia*, 33(6):635–645, 2017.

[15] James L B Robertson. The effects of image homogenisation on simulated transcranial ultrasound propagation. *Phys. Med. Biol*, 63(14):145014, 2018.

[16] David Attali, Thomas Tiennot, Mark Schafer, Elsa Fouragnan, Jérôme Sallet, Charles F Caskey, Robert Chen, Ghazaleh Darmani, Ellen J. Bubrick, Christopher Butler, Charlotte J Stagg, Miriam Klein-Flügge, Lennart Verhagen, Seung-Schik Yoo, Kim Butts Pauly, and Jean-Francois Aubry. Three-layer model with absorption for conservative estimation of the maximum acoustic transmission coefficient through the human skull for transcranial ultrasound stimulation. *Brain stimulation*, 16(1):48–55, 2023.

[17] Byung Gook Lee, Joon Jae Lee, and Jaechil Yoo. An efficient scattered data approximation using multilevel B-splines based on quasi-interpolants. *Proceedings of International Conference on 3-D Digital Imaging and Modeling, 3DIM*, pages 110–117, 2005.

[18] Jorge Nocedal and Stephen J. Wright. *Numerical Optimization.* Springer, New York, NY, USA, 2e edition, 2006.

[19] Nicolas Gengembre and Alain Lhémery. Pencil method in elastodynamics: Application to ultrasonic field computation. *Ultrasonics*, 38(1):495–499, 2000.

[20] Hamza Chouh, Gilles Rougeron, Sylvain Chatillon, Jean-Claude Iehl, Jean-Philippe Farrugia, and Victor Ostromoukhov. High performance ultrasonic field simulation on complex geometries. *AIP Conference Proceedings*, 1706(1):050002, 2016.

[21] Nicolas Gengembre. Pencil method for ultrasonic beam computation. *Proc. of the 5th World Congress on Ultrasonics*, 2003.

[22] Royer Daniel, Dieulesaint Eugène, Gennes Pierre-Gilles de, Daniel Royer, and Gennes Pierre-Gilles de. *Ondes élastiques dans les solides . Tome 1, Propagation libre et guidée / Daniel Royer,..., Eugène Dieulesaint,... ; préface de Pierre-Gilles de Gennes.* Enseignement de la physique. Masson, Paris, DL 1996.

[23] Jean-Francois Aubry, Oscar Bates, Christian Boehm, Kim Butts Pauly, Douglas Christensen, Carlos Cueto, Pierre Gélat, Lluis Guasch, Jiri Jaros, Yun Jing, Rebecca Jones, Ningrui Li, Patrick Marty, Hazael Montanaro, Esra Neufeld, Samuel Pichardo, Gianmarco Pinton, Aki Pulkkinen, Antonio Stanziola, Axel Thielscher, Bradley Treeby, and Elwin van 't Wout. Benchmark problems for transcranial ultrasound simulation: Intercomparison of compressional

wave models. *The Journal of the Acoustical Society of America*, 152(2):1003–1019, 2022.

[24] Samuel Pichardo, Vivian W. Sin, and Kullervo Hynynen. Multi-frequency characterization of the speed of sound and attenuation coefficient for longitudinal transmission of freshly excised human skulls. *Physics in Medicine and Biology*, 56(1):219–250, 2010.